Synthesis and Reactivity of Copper(I) Complexes based on C 3 - Symmetric Tripodal HTIM(PR 2) 3 Ligands

Ekaterina S Smirnova, Ferran Acuña-Parés, Eduardo Escudero-Adán, Christian Jelsch, Julio Lloret-Fillol

Synthesis and Reactivity of Copper(I) Complexes based on C_3-Symmetric Tripodal HTIM$(PR_2)_3$ Ligands

Ekaterina S. Smirnova, [a] Ferran Acuña-Parés, [a] Eduardo C. Escudero-Adán, [a] Christian Jelsch, [b] Julio Lloret-Fillol * [a, c]

[a] Institute of Chemical Research of Catalonia (ICIQ), The Barcelona Institute of Science and Technology, Avinguda Països Catalans 16, 43007 Tarragona, Spain. jlloret@iciq.es

[b] CRM2, UMR CNRS 7036, Institut Jean Barriol, Université de Lorraine, Vandoeuvre les Nancy CEDEX, France

[c] Catalan Institution for Research and Advanced Studies (ICREA), Passeig Lluïs Companys, 23, 08010, Barcelona (Spain)

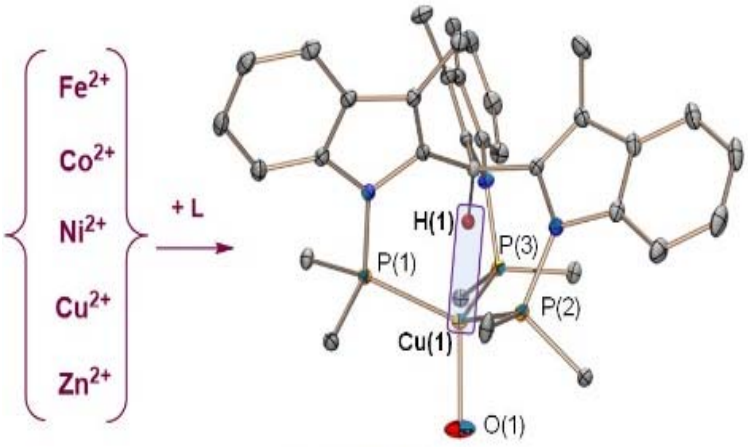

Abstract: We present the first example of a non-classical hydrogen bonding study for Cu^{I} complexes. To this end, we have studied the coordination capacity of the tripod phosphine ligands HTIM$(PR_2)_3$ (tris[1-(di-R-phosphino)-3-methyl-1*H*-indol-2-yl]methane, R = Ph, *i*Pr) leading to a series of eight Cu^{I} complexes [HTIM$(PR_2)_3$CuX] (R = Ph (**1-4**), *i*Pr (**5-8**); X = Cl^-, I^-, OTf^-, BF_4^-). A proposed anagostic interaction in the Cu^{I} complexes is based on ^{1}H NMR, experimental (Ultrahigh resolucion X-ray diffraction) and theoretical (Atoms-in-Molecules (AIM) and natural bonding orbital (NBO)) analysis of the electron density. Among the different synthesized complexes [HTIM$(PPh_2)_3$CuOTf] (**2**) showed the strongest Cu···H–C interaction with a linear geometry (179.98º) and the shortest well-described so far (*d*(Cu–H) = 1.9 Å) distance, in its toluene solvated form. Both parameters are characteristic for 3c-4e$^-$ interactions. In addition, we found that these tripodal ligands exhibit an unprecedented selectivity for Cu^{I} ions. The synthesized HTIM$(PR_2)_3Cu^{I}$ complexes have been found catalytically active and selective for the hydroboration of CO_2 to formic acid.

Introduction

Chemical reactivity and supramolecular structures are often governed by multiple weak (≤40 kcal·mol^{-1})[1] interactions. Among them, hydrogen bonding is one of the most important chemical interactions as it plays a central role in many physiological and biological processes.[2] The current accepted definition is that hydrogen bonds combine the interactions of three components: a hydrogen bond donor, a hydrogen bond acceptor and a hydrogen atom.[3] Usually hydrogen bonding involves the interaction of two electronegative *p*-block elements with a hydrogen atom. A more elusive situation is the participation of a transition metal in hydrogen bonding, which usually involves a polarized X–H bond.[2] This 3c-4e$^-$ interaction can be described by a donation of the filled *d*-orbital of the metal center into σ* orbital of the polarized X–H fragment and/or as the electrostatic interaction between partially positively charged hydrogen and a filled metal *d*-orbital (Figure 1).[4]

A better understanding of this non-classical hydrogen bonding can provide valuable information to determine the reaction intermediates involved in X–H bond activation mechanisms by metal centers. However, these type of interactions are difficult to study, especially for metal C–H anagostic interactions.[5] Indeed, the characterization of anagostic interactions are limited to rare examples, most probably due to the fact that they occur in reactive intermediates towards a C–H bond activation, making it challenging to stabilize them.[6] [3] Moreover, only few examples of first row transition metals featuring a three centers four electron bonding (3c-4e$^-$) have been reported.[6] [7]

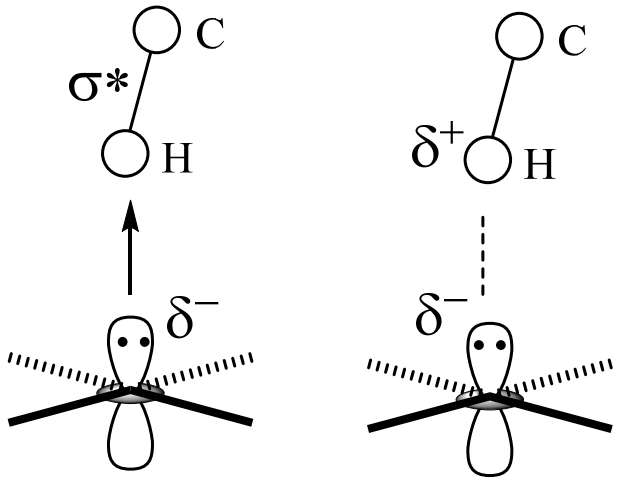

Figure 1. Attractive 3c–4e$^-$ M···HC hydrogen bonding in which the transition metal plays the role of a hydrogen-bond acceptor. (σ* stands for sigma antibonding orbital).

In 2006, the first example of a C_3-symmetric phosphorous-based tripodal ligand with a C-atom as an anchor (HTIM(PPh_2)$_3$, HTIM = tris[1-(diphenylphosphino)-3-methyl-1*H*-indol-2-yl]methane) (Figure 2) was reported.[8]

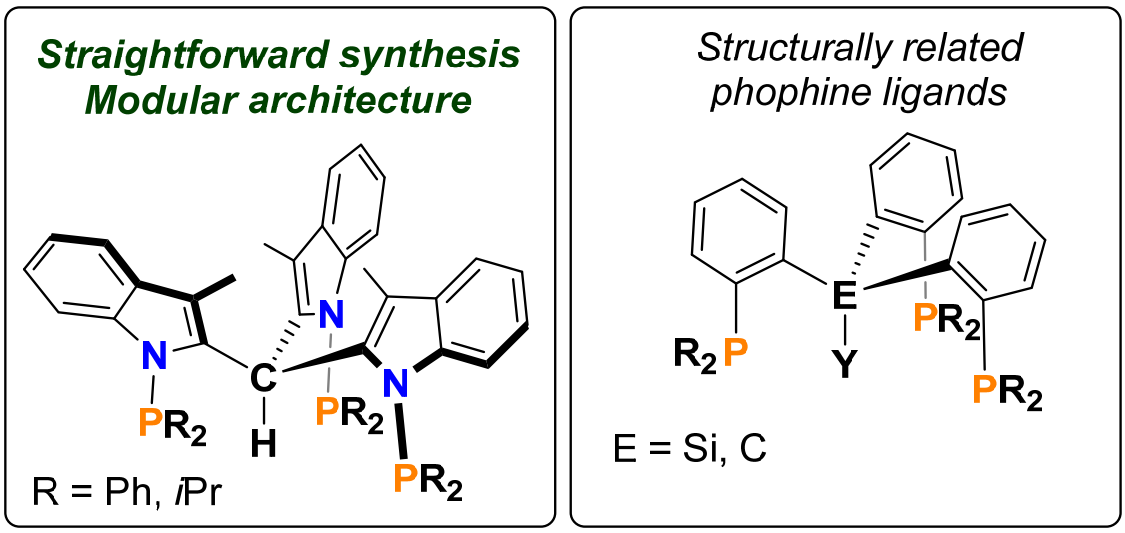

Figure 2. HTIM$(PR_2)_3$ ligands employed in this study (Left).Tripodal triphoshine ligands based on C and Si-anchor (Right).

The HTIM$(PPh_2)_3$ ligand has an unusual C_3 geometry, related to the highly versatile P_3^{SiH} [9] ((tris(2-R-(phosphaneyl)phenyl)silane) and P_3^{CH} [10] (tris(2-R-(phosphaneyl)phenyl)methane) ligands reported by J. Peters and co-workers (Figure 1) [9, 11] and P_3B (tris(2-R-(phosphaneyl)phenyl)borane) by D. Bourissou.[12] The unusual geometry of the P_3CH type ligands could potentially impose and force the formation of a non-classical (C–H)···M hydrogen bonding, allowing the study of exceptional (C–H)···M interactions. Despite its potential, there is only a single example of a X-ray diffraction structure, the HTIM$(PPh_2)_3$ molybdenum tricabonyl,[7] where (C–H)···M hydrogen bonding has been studied. To this end, we present herein the synthesis of a new HTIM$(PiPr_2)_3$ ligand, the atypical reactivity of HTIM$(PR_2)_3$ (R = Ph, *i*Pr) ligands with the first row transition metals along with the synthesis of copper complexes [HTIM$(PR_2)_3$CuX] (R = Ph; X = BF_4^- (**1**), OTf^- (**2**), Cl^- (**3**), I^- (**4**) and R = *i*Pr, X = BF_4^- (**5**), OTf^- (**6**), Cl^- (**7**), I^- (**8**)). Interestingly, we found a selective complexation of Cu^I ions by these tripodal ligands in presence of other first row transition metals.[13] The found selectivity can be rationalized by means of DFT calculations. This unique selectivity presents potential interest for copper salts separation or processing, since radioactive copper (^{64}Cu) is well-known for application in immuno-positron emission tomography (PET).[14],[15],[16]

We also have explored the capacity of the synthesized complexes to perform catalytic CO_2 hydroboration to study how the basicity of the ligand affects the reactivity. Copper complexes based on *N*-heterocyclic carbenes[17],[18],[19],[17],[20] and polyphosphine[21] ligands provide platforms to catalyze this interesting transformation from a fundamental point of view. Interestingly, copper complexes are among the few systems able to selectively reduce CO_2 to HCO_2BBN.[17] With respect to the development of new systems with the same selectivity pattern, it is important to establish the origin of the selectivity in order to advance in the development of synthetically useful transformations of CO_2.

Among the different synthesized complexes, [HTIM$(PPh_2)_3$CuOTf] (**2**) allowed for the first study of the non-classical (X–H)···M hydrogen bonding interaction in Cu^I complexes. We have characterized and further clarified the (C–H)···Cu interaction by a combination of experimental electron density map studies obtained by X-ray diffraction, Atoms-in-Molecules (AIM) and natural bonding orbital (NBO) analysis. This experimental and theoretical combination allows us to pinpoint the geometrical and electronic features of the (C–H)···Cu interaction in C_3-symmetric phosphorous-based tripodal system described herein.

Results and Discussion

Synthesis of HTIM(PR_2)$_3$ (R = Ph, *i*Pr) ligands and their reactivity with first row transition metals.

The modular HTIM(PPh_2)$_3$ ligand was synthesized by the reported procedure with a 75% yield.[8] We also developed the synthesis of the analogous more electron-rich phosphine HTIM(P*i*Pr$_2$)$_3$ bearing isopropyl substituents, which was isolated in 87% yield.

Both ligands show exceptional thermal stability and are robust with respect to oxygen and moisture. For instance, no traces of ligand oxidation/degradation were observed both after 24 h heating at 150 ºC in DMF (wet) or after being suspended in distilled water and left for 24 h in air.

The coordination ability of HTIM(PR_2)$_3$ ligands to first row transition metals is singular. For instance, the direct reaction of M(OTf)$_2$, MCl_2 (M = Fe, Ni, Co or Zn) with the HTIM(PPh_2)$_3$ and HTIM(P*i*Pr$_2$)$_3$ ligands does not yield any complex, even when forcing the reaction conditions to high temperature during an extended period of time (48 hours reflux in xylene). This is in contrast with the expected coordinating properties of tridentate phosphines, which typically react easily with metal salt precursors to form the respective complexes. We observed a different behavior when Cu^{I} salts react with HTIM(PPh_2)$_3$ and HTIM(P*i*Pr$_2$)$_3$ ligands. We can access different copper complexes (Scheme 1, **1-8**) by a direct reaction of appropriate metal salts ($Cu(MeCN)_4BF_4$, $Cu(MeCN)_4OTf$, CuCl and $(CuI)_4(SMe_2)_3$) with the ligand in dichloromethane at room temperature in less than 20 minutes, except for the CuCl precursor (18 h) due to a poor solubility in CH_2Cl_2.

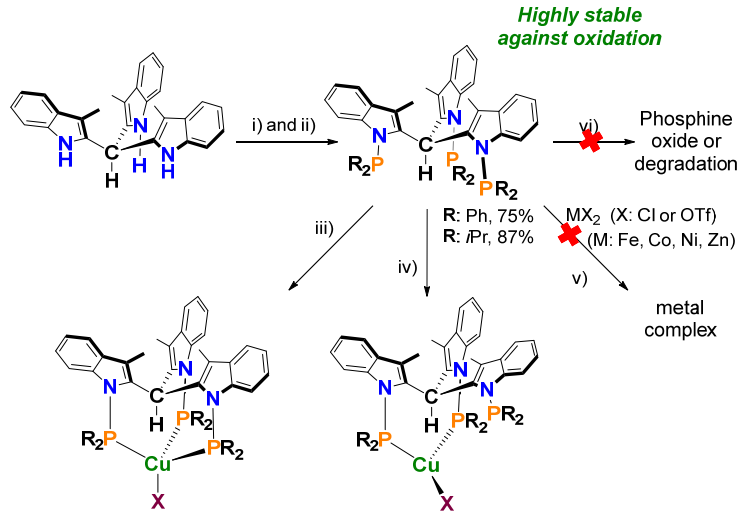

R = Ph, X = MeCN, BF_4^-, (89%) (**1**)
R = Ph, X = OTf^-, (87%) (**2**)

R = Ph, X = Cl^-, (84%, 70%*) (**3**)
R = Ph, X = I^-, (86%) (**4**)
R = *i*Pr, X = OTf^-, (86%) (**6**)
R = *i*Pr, X = Cl^-, (78%, 67%*) (**7**)
R = *i*Pr, X = I^-, (82%) (**8**)

R = *i*Pr, X = MeCN, BF_4^-, (85%) (**5**)

i) 3.5 equiv NaH, THF, 23 ºC; ii) 3.5 equiv **R**$_2$PCl, THF, 23 ºC;

iii) CH_2Cl_2, $Cu(MeCN)_4BF_4$ or $Cu(MeCN)_4OTf$, **R** = Ph;

iv) CH_2Cl_2, $Cu(MeCN)_4BF_4$ or $Cu(MeCN)_4OTf$ or $(CuI)_4(SMe_2)_3$ or CuCl or $CuCl_2$, **R** = Ph; *i*Pr

v) CH_2Cl_2 (rt) or toluene (110 ºC) or xylene (135 ºC) or MeCN (80 ºC)

vi) toluene, 110 ºC or xylene, 130 ºC or 10 bar O_2, MeCN, 80 ºC, or H_2O, air, DMF, 150 ºC, all 24 - 36 h

Scheme 1. Modular synthesis of HTIM(PR_2)$_3$ (R = Ph, *i*Pr) ligands, and new copper(I) complexes with HTIM(PR_2)$_3$ phosphines.

Remarkably, the reaction of $Cu^{II}Cl_2$ with the phosphines ($HTIM(PR_2)_3$ (R = Ph, *i*Pr)) in MeOH under air atmosphere yielded the same copper complexes (**3** and **7**, respectively), with similar yields as when starting from $Cu^{I}Cl$ (70% to 84% in case of **3** and 67% to 78% for **7**). Nevertheless, when starting from the $Cu^{II}Cl_2$ salt the reaction was faster (less than 20 min). A titration experiment in an NMR tube of $HTIM(P\textit{i}Pr_2)_3$ with $Cu^{II}Cl_2$ in CD_3OD indicates that the reaction is stoichiometric. Half of an equivalent of $CuCl_2$ leads to a 1:1 mixture of $HTIM(P\textit{i}Pr_2)_3$: complex **7**, while 1 equiv of $CuCl_2$ cleanly form complex **7** and no further changes were observed upon further $CuCl_2$ addition (Figure SI-1). The easy formation of the Cu^{I} complexes can be ascribed to the high stability of Cu^{I} complexes and due to the fact that Cu^{II} to Cu^{I} reduction is facilitated by methanol.

Figure 3. ORTEP plots (50% probability ellipsoids) of the complex **1** (d (Cu–P) = 2.3158(8)–2.4133(9), d (Cu···H) = 1.994 Å), **2** (d(Cu–P) = 2.3056(4)–2.3759(4), d(Cu···H) = 1.934 Å), **3** (d(Cu–P) = 2.2339(5)–2.2551(5), d(Cu···H) = 2.328 Å), **7** (d(Cu–P) = 2.2657(5)–2.2687(5), d(Cu···H) = 2.232 Å), Ph and *i*Pr substituents, CH_3CN are simplified to C-atom, OTf^- to O-atom, non-coordinating anions are omitted for clarity.

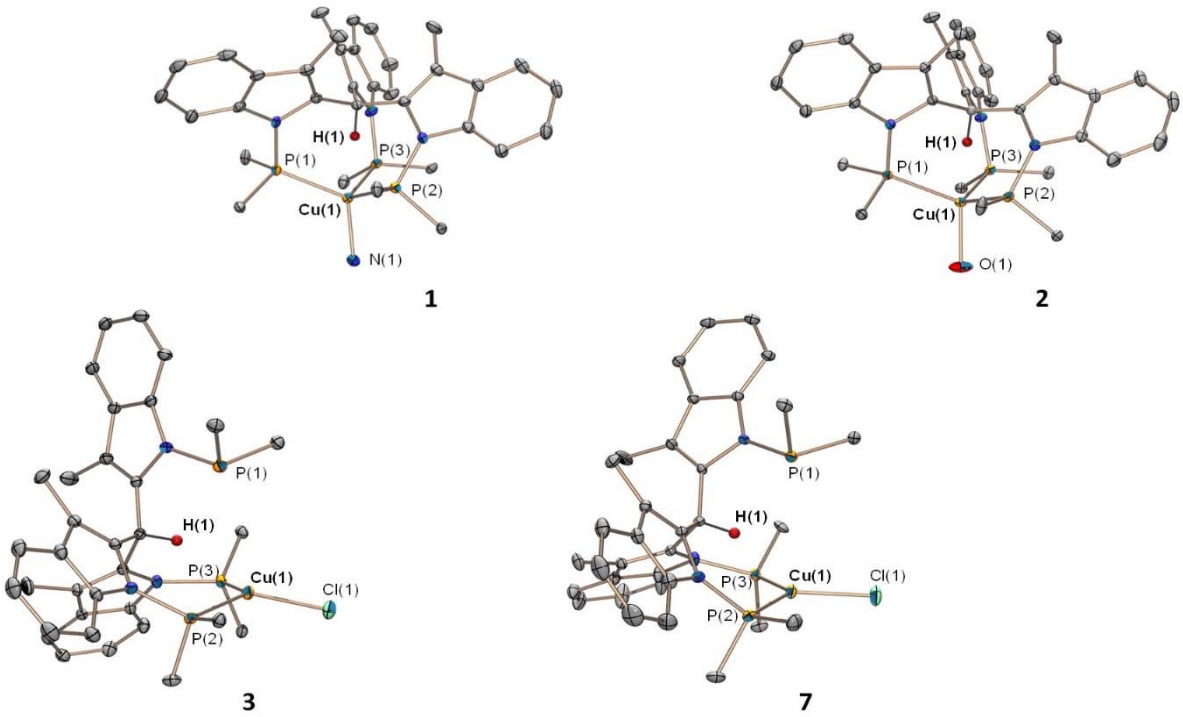

In addition it is an indication of the capacity of the ligand to stabilize low oxidation states of Cu^{I} that is known to adapt to several coordination geometries.

In total, eight new complexes have been synthesized and were

characterized both in the solid state and in solution (Scheme 1, Figure 3) by polynuclear NMR spectroscopy, HRMS and X-ray diffraction analysis, except for complexes **5** (the obtained X-ray data was not good enough for CIF though we can confirm κ^2-coordination mode of the ligand) and **8**.The

obtained complexes do not degrade with time being kept under ambient conditions and no traces of decomposition were observed after their solutions in MeCN-d_3 were refluxed for 24 h. The solid state analysis shows two different triphosphine coordination geometry environments. For stronger binding anions such as Cl^- or I^- and the HTIM(P*i*Pr$_2$)$_3$ ligand, a phosphorous atom κ^2-coordination mode was observed while C_3 symmetric complexes were obtained only in the case of weakly coordinating anions or solvent molecules like CH_3CN with HTIM(PPh_2)$_3$ ligand. Beside the (C–H)···Cu^I hydrogen bonding interaction, which will be discussed later in more detail, the other geometric parameters are in the expected ranges.

Ligand coordination selectivity. We tested the unusual selectivity towards the formation of the copper complexes by reacting the HTIM(P*i*Pr$_2$)$_3$ ligand with a pool of metal-triflates: Fe^{2+}, Ni^{2+}, Co^{2+}, Cu^+ and Zn^{2+} salts in CD_2Cl_2:CD_3CN (3:1). The only detected compound by $^{31}P\{^1H\}$ NMR and ESI-HRMS was [(P- HTIM(PR_2)$_3$)Cu(CD_3CN)]$^+$ (see SI for details: Figure SI-2 and Figure SI-3). Moreover, under biphasic reaction conditions, the reaction of Fe^{2+}, Ni^{2+}, Co^{2+}, Cu^{2+} and Zn^{2+} chlorides in water with HTIM(P*i*Pr$_2$)$_3$ in organic solvent (CD_2Cl_2, EtOD (10 % v/v)) at room temperature and under air atmosphere exclusively leads to the formation of [(HTIM(P*i*Pr$_2$)$_3$CuCl]. From the organic phase, we selectively isolated [(HTIM(P*i*Pr$_2$)$_3$)CuCl] (**7**) from a metal chloride salt pool in 67% yield (Figure 4 and see SI: Figure SI-4), the purity of the compound has been proved by elemental analysis: (%) calculated for [$C_{46}H_{64}CuN_3P_3Cl$] C% 64.93, H% 7.58, N% 4.94; found C% 64.74, H% 7.37, N% 5.04. To the best of our knowledge, this marked selectivity is unpreceded for phosphine ligands.
The selectivity observed is in agreement with the Irving-Williams series of relative complex stabilities of first row divalent metal ions, which identifies Cu^{2+} as the most stable ion that may be attributed to the Jahn-Teller distortion. [13a, 22] [13a, 23] Nevertheless, it is difficult to explain the absence of reactivity with other M^{2+} salts.

The origin of this unusual reactivity may involve a balance between metal-phosphorous binding energy and ligand reorganization energy due to coordination. To get some insights in the effect of these energetic contributions, we compared DFT calculations on complexes of both copper and nickel with HTIM(PPh_2)$_3$ (including dispersion and solvent effects, See SI for complete computational details).

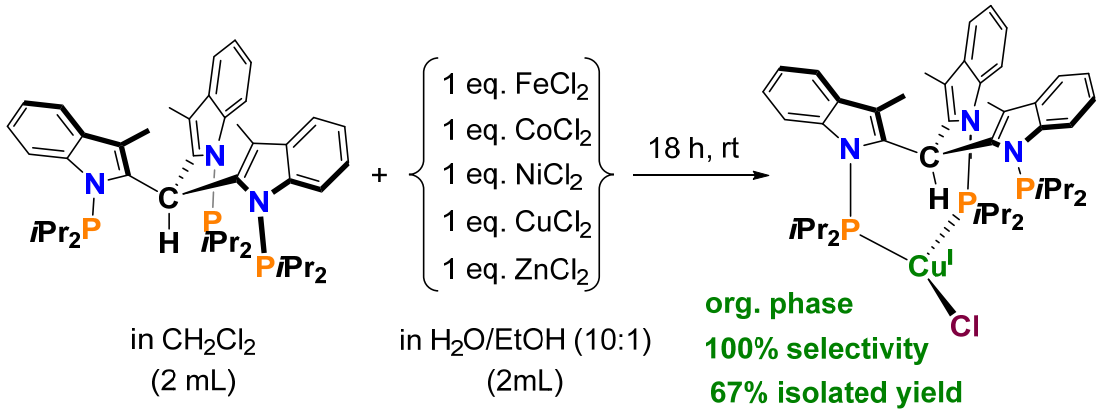

Figure 4. Selective formation of complex [(κ^2*P*-HTIM(P*i*Pr$_2$)$_3$)CuCl] in the presence of Fe^{2+}, Ni^{2+}, Co^{2+}, Cu^{2+} and Zn^{2+} chlorides.

Therefore, we first located the possible copper and nickel coordination isomers with the HTIM(PPh_2)$_3$ ligand. For both metals, the coordination isomer most stable with HTIM(PPh_2)$_3$ is the di-coordinated one, ([(κ^2P-HTIM(PPh_2)$_3$)Cu(CH_3CN)]$^+$ and [(κ^2*P*-HTIM(PPh_2)$_3$)Ni(CH_3CN)$_2$]$^{2+}$ (Figures SI-5B,5D). Interestingly, the thermodynamics of the [(κ^2*P*-HTIM(PPh_2)$_3$)Cu(CH_3CN)]$^+$ formation is clearly exergonic (-16.5 kcal·mol^{-1}), but for [(κ^2*P*-HTIM(PPh_2)$_3$)Ni(CH_3CN)$_2$]$^{2+}$ is virtually isoenergetic. The formation energy favors [(κ^2*P*-HTIM(PPh_2)$_3$)Cu(CH_3CN)]$^+$, by c.a. 15 kcal·mol^{-1}, in agreement with the experimental high selectivity for the copper complex. The ligand reorganization energy, calculated as the energy difference between the free ligand and in the coordination geometry, is 5.4 and 9.8 kcal·mol^{-1} for the copper and nickel complexes, respectively. The smaller reorganization energy for the copper complex can be rationalized by comparing the M–P distances (d(Cu–P)$_{aveg}$ and d(Ni–P)$_{aveg}$ of 2.24 Å and 2.36 Å, respectively), suggesting that coordination to the smaller metal ion is favored by 4.4 kcal·mol^{-1}. We also estimate the metal-phosphorus binding energy,[24] which is more favorable for the copper(I) than for the nickel(II) complex by 8.9 kcal·mol^{-1}, again in line with the experimental selectivity. Based on our computational results, we can rationalize that both, the ligand distortions and binding energy play an important role in the selectivity. This selectivity may be exploited in the separation or processing of radioactive copper salts (^{64}Cu), well-known as immuno-positron emission tomography (PET) agent.[25] [26]

Coordination behaviour in solution.

Complexes **1** and **2** present a singlet in the ^{31}P{^{1}H} spectrum at room temperature as expected by the *C*$_3$ κ^3*P*-coordination mode is the solid state. The ^{1}H NMR signals only suffers a signal broadening upon cooling down to 183 K. interestingly, complex **3, 6** and **7** follows the same behavior despite the fact that presents a κ^2*P* coordination mode in the X-ray diffraction structure.

Complex **4** shows a broad signal in the ^{31}P{^{1}H} spectrum at room temperature, suggesting a dynamic behavior (Figure 5). Indeed, NMR temperature dependent studies revealed the transformation of the broad ^{31}P{^{1}H} signal into a multiplet at low temperature. Unfortunately, the multiplet is not fully resolved even at 183 K, which makes it difficult to draw conclusions. Clearer is the behaviour of complex **8**, where the sharp singlet at room temperature is transformed into two doubles and a singlet with relative integration 1:1:1 in the ^{31}P{^{1}H} NMR, strongly suggesting the κ^2*P*-ligand coordination mode in solution at 183 K as in the X-ray diffraction structure. In the case of complexes **6** the appearance of two doublets was also observed (Figure SI-7).

The general observed singlet in ^{31}P{^{1}H} spectra at room temperature is consistent with a κ^3*P*-coordination expecially for those systems that do not present a two doublet and a singlet with 1:1:1 ^{31}P{^{1}H} NMR integration pattern. Nevertheless, we can not discard a fast equilibrium between the three possible C_2-symmetric Cu^I coordinations at room temperature.

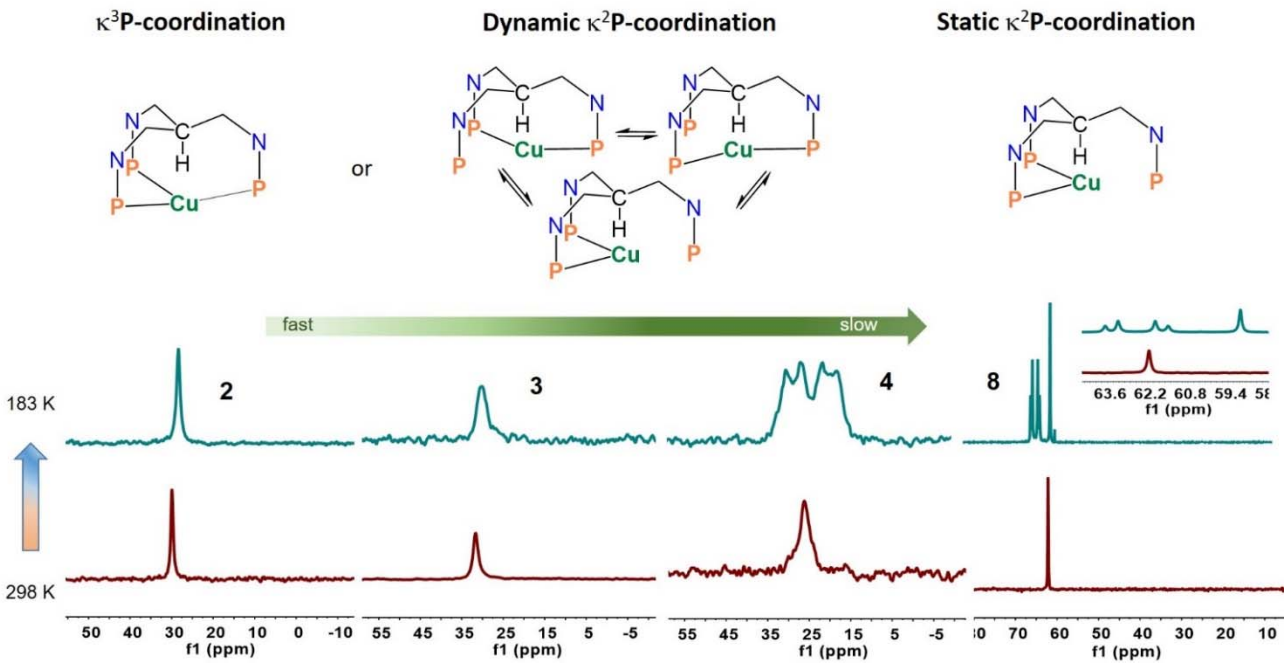

Figure 5. a) T correlation $^{31}P\{^{1}H\}$ NMR studies for complex **2** - **4** and **8** (CD_2Cl_2, 298 and 183 K)**.**

Catalytic CO_2 reduction to HCO_2BBN.

We next investigated the catalytic activity of our copper complexes in the hydroboration of CO_2 which is challenging due to the high enthalpy (127.3 $kJ \cdot mol^{-1}$) of C=O double bond and which frequently presents kinetic difficulties. However, it has been reported that complexes based with polydentate phosphine ligands can catalyze this transformation using strong reducing agents. In particular, tridentate Cu^{I} complexes habe been shown very effective.[17, 27] We observed that complexes **1**-**4** containing Ph substituents on the phosphorous atoms are active and selective catalysts for CO_2 to HCO_2BBN in THF-d_8 (In $CDCl_3$ the catalytic activity drops (see SI, table SI-1)) with TON values in the range of 20 – 22. We discard the formation of compounds methoxy-BBN (**C**) and BBN ether (**D**) since were not detect by ^{1}H NMR.

Table 1. CO_2 hydroboration catalytic tests.

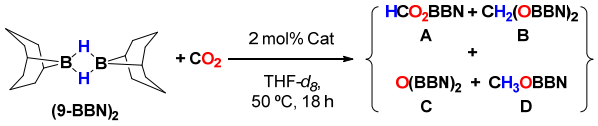

Entry	Catalyst	Selectivity (A/B)	TON
1	**HTIM(P*i*Pr$_2$)$_3$**	100:0	≤2
2	**HTIM(PPh$_2$)$_3$**	100:0	≤2
3	**Cu(MeCN)$_4$OTf**	100:0	≤2
4	**CuCl**	100:0	≤2
5	**Cu(MeCN)$_4$BF$_4$**	100:0	≤2
6	**1**	100:0	19
7	**2**	97:3	22
8	**3**	95:5	20
9	**4**	99.1	20
10	**5**	98:2	22
11	**6**	97:3	22
12	**7**	99:1	25
13	**8**	99:1	31

Reaction conditions: CO_2 (1 atm), $(9\text{-BBN})_2$ (0.09 mmol), Catalyst (2 mol%). Yield and selectivity determined by ^{1}H NMR using mesitylene as the internal standard.

At the end of the reaction, only a signal corresponding to the free ligand was observed in the $^{31}P\{^1H\}$ NMR, showing that the Cu metal decoordinates during catalysis. The formation of a metallic mirror on the wall of the reaction tube, suggests the formation of metallic copper. In contrast, complexes with the *i*Pr substituted phosphines, with sightly higher catalytic activity (22 – 31 TON), remain intact after catalysis. The absence of clear differences between the different complexes among the series with $HTIM(PPh_2)_3$ may be again an indication of a similar coordination geometry in solution of these complexes that will be discussed later.

The selective formation of HCO_2BBN is interesting from a fundamental point of view. The number of catalysts that can selectively reduce CO_2 to HCO_2H is rather limited.[17] Consequently, the development of new catalysts for this transformation is relevant to establish origins of the selectivity and to advance in the development of synthetically useful transformations for CO_2 functionalization.

Experimental and theoretical characterization of the Csp^3–H···Cu interaction. We have studied the (C–H)···Cu^I interaction by X-ray diffraction analysis, ^{1}H-NMR and computational modelling at DFT level (see SI for Computational details).

A careful inspection of the Cu···H distances by X-ray diffraction data in comparison with the DFT calculations showed a good geometric match. The analysis reveals that Cu···H–Csp^3 distance falls in the 1.9–2.3 Å range, and most of the structures have an angle close to 180°. The previous geometrical features are consistent with a possible 3c-4e$^-$ interaction.

The shortest Cu···H–Csp^3 distances were found for complexes **1** and **2**, which present a κ^3*P*-coordination mode (1.934 Å for **2** and 1.994 Å for **1**, Figure 6), in good agreement with the calculated

distances (Table 2). A Natural Bond Orbital (NBO) analysis[28][14] for the selected compounds indicate that a charge donation occurs from the Cu^{I} to the C–H bond ($\Delta q(H) < 0$). The intramolecular charge transfer decreases with the theoretical Cu···H distance (Table 2). The donor-acceptor delocalization energies from the copper orbitals to the $\sigma^*_{C\text{-}H}$ orbital in complex **2** is remarkable (16.3 kcal·mol^{-1}) and the $\sigma_{C\text{-}H}$ orbital to the copper (ΔE_{total} ($\sigma_{C\text{-}H} \rightarrow n_{Cu}$)) are significantly lower than those reported for agostic interactions,[15] suggesting the anagostic character of the Cu···H–Csp^3 interaction.

Likewise, we have also inspected the ^{1}H-NMR of the Csp^3–H proton. In CD_2Cl_2 solution, we observed a down-field shift for all synthetized complexes compared to the free Csp^3–H proton (Figure 6),[5e, 29] which is consistent with previously studied non-classical hydrogen bonding in d^8 complexes.[6-7] For the less donating and bulky substituents (HTIM(PPh$_2$)$_3$ ligand), the deshielding effect is more than 1.5 ppm in comparison with the free phosphine ligand (8.7 ppm (q, CD_2Cl_2)), while for the HTIM(P*i*Pr$_2$)$_3$ tripod phosphine, a small shift of 0.6 ppm is observed.

Table 2. Summary of the Cu^{I}-H and Csp^3-H bond distances (Å), the ^{1}H chemical shift of the Csp^3-H moiety (δ: ppm) and the proton chemical shift change upon complexation ($\Delta\delta$: ppm), the NPA charge transferred from the metal to the H–Csp^3 bond (Δq: a.u. units), the total donor-acceptor interaction energy (ΔE_{total} ($\sigma_{C\text{-}H} \rightarrow n_{Cu}$): kcal·mol^{-1}), the bond critical point parameters of the Cu^{I}··H interaction ($\rho(\mathbf{r})$, $\nabla^2\rho(\mathbf{r})$, $G(\mathbf{r})$, $V(\mathbf{r})$, and $H(\mathbf{r})$ in a.u.) and its energy (ΔE_{HB}: kcal·mol^{-1}) for selected copper complexes.

[a]ref. 15. [b] $\Delta\delta(H) = \delta_{(H)\ complex} - \delta_{(H)\ free\ ligand}$. [c]$\Delta q(H) = q(H)_{complex} - q(H)_{free\ ligand}$. [d] The hydrogen bond interaction energy is computed as $\Delta E_{HB} = 0.5 * V(r) * 627.51$. [e] Cu^{I}···H bond critical point properties derived from high-resolution X-ray diffraction data.

exp. (calc.)	**2**	**7**
$d_{(H\text{-}C)}$	1.092 (1.098)	0.980(1.100)
$d_{(H\cdot\cdot Cu)}$	1.934 (1.904)	2.231(1.998)
$\delta_{(H)}$	10.8 (11.3)	8.05(8.6)
$\Delta\delta_{(H)}$[b]	2.1(2.3)	0.55(1.0)
$\Delta q(H)$[c]	-0.11	-0.09
ΔE_{total} ($\sigma_{C\text{-}H} \rightarrow n_{Cu}$)	6.2	6.3
$\rho(\mathbf{r}_{cp})$	0.030 (0.044)	-0.034
$\nabla^2\rho(\mathbf{r}_{cp})$	-0.039 (-0.032)[e]	(-0.028)
$G(\mathbf{r}_{cp})$	0.036 (0.040)[e]	-0.032
$V(\mathbf{r}_{cp})$	-0.030 (-0.088)[e]	(-0.071)
$H(\mathbf{r}_{cp})$	0.005 (-0.048)[e]	(-0.039)
ΔE_{HB}[d]	-27.6	-22.3

Figure 6. C–H···Cu distances, Å (X-ray data), top scheme; δ Csp^3–H (CD_2Cl_2), bottom scheme.

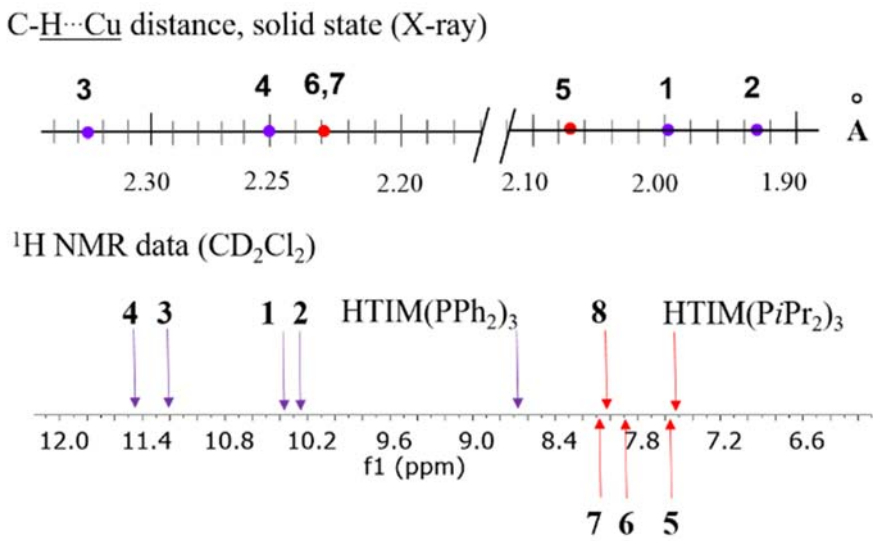

Figure 7. Contour diagrams in the Cu-H-Csp^3 plane for complex **2'** for: experimental model deformations of the electron density top-right) dynamic (F_{mult} - F_{sph}), top-left) Static (ρ_{mult} - ρ_{sph}), bottom-right) experimental Laplacian map, botton-left) DFT Laplacian map, $-\nabla^2\rho(r)$. (red regions represent negative values, while blue regions represent positive values).

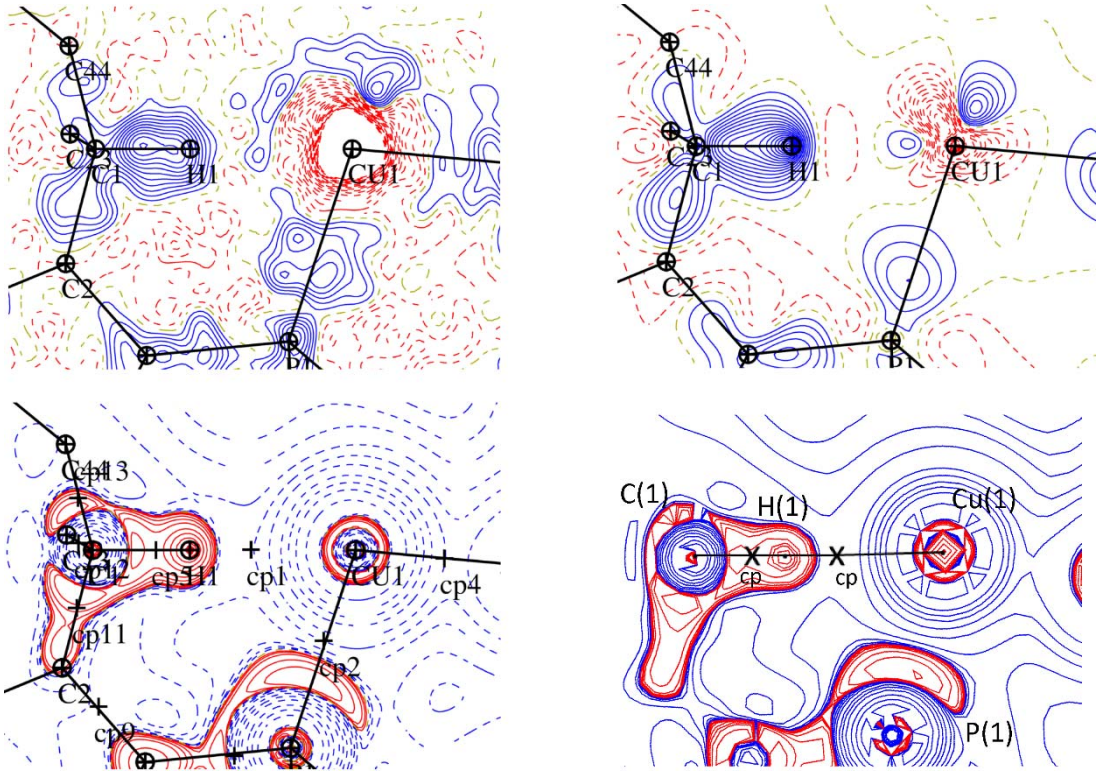

The DFT data are again in good agreement with the experimental results; nevertheless the predicted deshielding effect is in general larger by c.a. 0.5 ppm. (Table 2).

It is worth to mention that in the gradient temperature studies for complexes **3** and **4** (Figure SI-8) in the ^{1}H NMR experiment, the characteristic pattern of downfield shifting with lowering temperature that has been described in the literature[6] for anagostic interactions stopped at 213 K. Due to this slowing down in the exchange of Cu^{I} coordination to the phosphorous atoms of the ligand, we observed a decrease in deshielding effect of the Csp^3–H proton (Figure SI-8).

The experimental charge density was refined using the Hansen & Coppens multipolar atom model with program MoPro[30]. X-H distances were constrained to standard neutron diffraction values.[31] The C1-H1 distance was set to d=1.099 Å. The Cu atom was modelled up to hexadecapole level. Using this model, the X-ray structure of **2** with toluene solvate (**2'**) resulted in a very low R-factor of 1.890%. (Table 2).

The experimental Laplacian density (Figure 7) map and the $Cu^{I}\cdots H$ bond critical point properties of complex **2'** were obtained from high-resolution X-ray diffraction data and compared with the theoretical ones.The Atoms in Molecules (AIM) theory was applied to both models (Figure 7).[21] The two approaches reveal the existence of a $Cu^{I}\cdots H$ bond path interaction. The deformation electron density show a small electron accumulation on the copper atom towards the H1 atom, while the density is depleted in the direction of the phosphorous atoms.

The experimental and DFT approaches present similar Laplacian contour maps. Density Functional Theory underestimates the $V(r)$ and $H(r)$ values, but $\rho(\mathbf{r})$, $\nabla^2\rho(\mathbf{r})$ and $V(\mathbf{r})$ are in good agreement with the X-ray derived parameters (Table 2). The slight divergences may have their origin in the inaccurate modelling of the non-covalent interactions at this level of theory. Thus, both analyses show a $Cu^{I}\cdots H$ interaction described as a 3c-4e^{-} anagostic bonding with partial covalent character.

Conclusions

The first systematic study of the (C–H)$\cdots Cu^{I}$ intramolecular interaction in a newly synthesized family of copper complexes based on C_3 symmetric tripodal ligands is reported. Experimental data indicate that the HTIM$(PR_2)_3$ ligands exclusively coordinate with Cu^{I} in presence of other first row transition metals in the oxidation state (II). DFT calculations predict that the coordination ability has its origin in the lower phosphorus binding energy and ligand reorganization energy required to capture small metal cations such as Cu^{I}. This behavior may be used in analytical cation separation procedures.

Crystallographic and ^{1}H-NMR data reveal that these systems present different κP-coordination modes according to steric effects of the *i*Pr and Ph groups and counterion identity. A careful analysis of the geometrical features and of the electronic structure of these complexes suggests that the (C–H) $\cdots Cu^{I}$ contact is best described as a 3c-4e^{-} anagostic interaction with partial covalent character. The charge donation from the metal to the C–H bond is more

pronounced for copper systems with a κ^3P-coordination mode due to the shorter Cu···H distances, leading to a pronounced downfield displacement of the Csp^3–H···Cu^I proton signal. The interplay between the binding affinity, the ligand reorganization energy and the geometrical parameters that facilitate the Cu···H contact should be considered to analyze the impact of this interaction in the X–H bond activation mechanisms

Experimental Section

General Procedures. Unless otherwise mentioned, all reactions were performed under a N_2 atmosphere using standard Schlenk techniques or conducted after preparation in the glove box. Anhydrous solvents for synthesis were obtained by passing them through an activated alumina column on a PureSolvTM solvent purification system (Innovative Technologies, Inc., MA). Deuterated solvents were purchased from Sigma-Aldrich. NMR spectra were recorded either on a Bruker Avance 400 or 500 Ultrashield instruments. The chemical shifts (δ, ppm) were referenced to residual solvent resonances and external 85% H_3PO_4 in the ^1H and $^{31}P\{^1H\}$ spectra, respectively. Coupling constants (J) are reported in hertz (Hz). Mass spectra were recorded on a Water LCT Premier Spectrometer (ESI and APCI), on an Autoflex Bruker Daltonics (MALDI and LDI), or on an AgilentMSD-5975B (GC-MS). Elemental analyses were performed on a LECO CHNS 932 microanalyzer at the Universidad Complutense (Madrid). Crystal structure determinations were carried out using a MM-007HF diffractometer equipped with an Pilatus 200K hybrid pixel detector, a rotating anode for Mo $K\alpha$ radiation and Oxfrod Cryostream 700 plus low temperature device (T = – 183º C). Full-sphere data collection was used with ω scans. Programs used: Data collection and data reduction, CrysAlisPro 1.171.39.12b[32] and absorption correction SADABS-2014/5.[33] Structure Solution and Refinement: Crystal structure solution was achieved using the VLD procedure implemented in SIR2014[34]. Spherical model refinement was done using the program ShelXle[35]. All non-hydrogen atoms were refined including anisotropic displacement parameters. Copper(I) chloride, copper(II) chloride, copper(I) tetrakis(acetonitrile)triflate, copper(I) tetrakis(acetonitrile)tetrafluoroborate, diphenyl-phospine chloride (99% purity), diisopropylphosphine chloride (98% purity) were purchased from Merck (Sigma-Aldrich) and used without further purification. Unless otherwise stated, all other reagents were purchased from commercial sources and used without further purification.

Supplementary crystallographic data for the structures contained in this paper have been deposited in the Cambridge Crystallographic Data Centre with numbers CCDC-1829080 (compound **HTIM(PiPr$_2$)$_3$**), CCDC-1829088 (compound **1**), CCDC-1829083 (compound **2**), CCDC-1829078 (compound **2'**), CCDC-1829087 (compound **3**), CCDC-1829077 (compound **4**), CCDC-1829081 (compound **7**) and CCDC-1829084 (compound 8).

Synthesis of tris(*N*-diisopropylphosphino-3-methyl-2-indolyl)methane (HTIM(P*i*Pr$_2$)$_3$). The ligand was synthesized by the modified protocol of the synthesis of tris(*N*-diphenylphosphino-3-methyl-2-indolyl)methane. The tris(3-methyl-2-indolyl)methane (2.00 g, 4.95 mmol) in 70 ml of THF was added to a stirred solution of washed NaH (416.00 mg, 17.33

mmol, 3.5 equiv) in THF (60 ml) at 23 ºC during 15 min. After vigorous stirring at 50 ºC for 1.5 h, the solution was cooled down to 23 ºC. A solution of ClP*i*Pr$_2$ (98% purity) (2.76 mL, 17.33 mmol, 3.5 equiv) in THF (50 mL) was added dropwise and the reaction mixture was stirred at 23 ºC over a period of 16 h. The resulting reaction mixture (yellow-orange) was filtrated under nitrogen flow and the resulting orange filtrate was concentrated in vacuum to 20 mL. Addition of dry MeCN (100 mL) resulted in the immediate formation of the crystalline white precipitate which could be separated by filtration under air on the membrane pump. The new tripode phosphine was found to be soluble in chlorinated alkane solvents, diethyl ether, toluene, hexane and alcohols. Yield 3.25 g, 4.31 mmol (87%). Once precipitated from the reaction mixture, a new ligand can be kept in the presence of moisture and air without any traces of degradation.

^{1}H NMR (500 Hz, $CDCl_3$) *δ* 7.53−7.51 (m, 3H), 7.48 (q, 1H, $^4J_{H\text{-}P}$ = 5.1 Hz), 7.41−7.40 (m, 3H), 7.15−7.07 (m, 6H), 2.79 (sept, *J* = 4.2 Hz), 1.67 (s, 9H), 1.32−1.26 (m, 9H), 1.17−1.13 (m, 9H), 0.89−0.84 (m, 9H), 0.42−0.38 (m, 9H). **^{1}H NMR** (500 Hz, CD_2Cl_2) *δ* 7.55−7.53 (m, 3H), 7.50 (q, 1H, *J* = 5.1 Hz), 7.41−7.38 (m, 3H), 7.15−7.05 (m, 6H), 2.80 (sept, *J* = 4.2 Hz), 1.67 (s, 9H), 1.33−1.27 (m, 9H), 1.17−1.12 (m, 9H), 0.90−0.84 (m, 9H), 0.42−0.37 (m, 9H). **^{31}P{^{1}H} NMR** (202.5 Hz, $CDCl_3$) *δ* 60.54 (s). **^{31}P{^{1}H} NMR** (202.5 Hz, CD_2Cl_2) *δ* 61.13 (s). **^{13}C NMR** (125 Hz, $CDCl_3$) *δ* 140.6 (s, C), 139.2 (s, C), 132.4 (s, C), 121.6 (s, CH), 119.6 (s, CH), 118.6 (s, CH), 115.8 (s, C), 113.3 (s, CH), 38.6 (q, $^3J_{C\text{-}P}$ = 22.5 Hz, H–$\underline{C}_{sp3}$), 28.3−27.5 (m, CH3), 22.6−22.1 (m, CH_3), 20.2−19.3 (m, CH_3), 9.3 (s, CH_3). **^{13}C DEPTQ NMR** (125 Hz, CD_2Cl_2) *δ* 141.2 (m, C), 140.9

(s, C), 139.7 (s, C), 132.8 (s, C), 121.1 (s, CH), 119.9 (s, CH), 118.9 (s, CH), 116.2 (s, C), 113.8 (s, CH), 39.0 (q, $^3J_{C\text{-}P}$ = 28.8 Hz, H–$\underline{C}_{sp3}$), 28.0−27.8 (m, CH3), 23.2−22.8 (m, CH_3), 22.5 (s, CH_3), 22.2 (s, CH_3), 20.4 (s, CH_3), 20.1 (s, CH_3), 19.6−19.5 (m, CH_3), 9.4 (s, CH_3). **HRMS** (ESI, MeOH): calculated for $[C_{46}H_{65}N_3P_3]^+$, [M+H$^+$]: 752.4386; found: 752.4356. **X-Ray** quality crystals were obtained by slowly cooling down to 23 ºC a concentrated solution of **HTIM(P*i*Pr$_2$)$_3$** in acetonitrile.

General procedure for the synthesis of Cu^I complexes: To a 5 mL solution of HTIM(PPh_2)$_3$ or HTIM(P*i*Pr$_2$)$_3$ (150.00 mg or 120.00 mg, 0.16 mmol) in CH_2Cl_2 (SPS grade) was added a solution of the corresponding copper salt (0.161 mmol) in CH_2Cl_2 (2 mL). Reaction was usually completed within 30 min, except for CuCl (reaction mixture was left overnight due to the insolubility of CuCl in CH_2Cl_2). For $CuCl_2$, 0.8 mL of MeOH were used instead. All obtained complexes can be isolated by recrystallization in air from the concentrated reaction mixture by addition of *t*BuOMe or hexane or by slow diffusion of diethyl ether. For the systematic studies, due to the low solubility of some compounds in $CDCl_3$, all NMR data were obtained in CD_2Cl_2 purchased from Merck (Aldrich).

[HTIM(PPh$_2$)$_3$Cu(NCMe)]BF$_4$ (1). Yellowish crystalline solid obtained in 89 % by recrystallization from CH_2Cl_2:*t*BuOMe. **^{1}H NMR** (400 Hz, CD_2Cl_2) *δ* 10.37 (q, 1H, $^4J_{H\text{-}P}$ = 12.6), 7.53−7.50 (m, 3H), 7.40−7.36 (m, 3H), 7.31−7.22 (m, 15H), 7.06 (t, *J* = 8.0 Hz, 3H), 6.96 (t, *J* = 8.0 Hz, 6H), 6.71 (t, *J* = 8.5 Hz, 3H), 6.61−6.57 (m, 6H), 6.34−6.32 (m, 3H), 2.11 (s, 9H), 1.90 (s, 3H, C$\underline{H}_3$CN); **^{31}P{^{1}H} NMR** (162 Hz, CD_2Cl_2) *δ* 31.40 (s); **^{13}C NMR** (101 Hz, CD_2Cl_2) *δ*

139.3−139.2 (m, C), 136.8−136.6 (m, C), 133.2 (s, C), 131.2−130.9 (m, CH), 130.4 (s, CH), 129.9−129.7 (m, CH), 129.3−129.2 (m, CH), 123.2 (s, CH), 121.9 (s, CH), 119.7 (s, CH), 119.3 (s, C), 116.0 (s, C), 37.5 (q, $^{3}J_{C\text{-}P}$ = 21.2 Hz, H–$\underline{C}_{sp3}$), 8.9 (s, CH_3), 2.2 (s, CH_3); **^{19}F{^{1}H} NMR** (376 Hz, CD_2Cl_2) *δ* – 149.02 (s). **HRMS** (ESI, MeOH): calculated for $[C_{64}H_{52}CuN_3P_3]^+$, [M-MeCN-BF_4]$^+$: 1018.2665; found: 1018.2655. **X-Ray** quality crystals were obtained by slow diffusion of *t*BuOMe into the solution of the **1** in CH_2Cl_2 at 23 ºC.

[HTIM(PPh$_2$)$_3$Cu]OTf (2). Yellowish crystalline solid obtained in 87 % by recrystallization from CH_2Cl_2:*t*BuOMe. **^{1}H NMR** (400 Hz, CD_2Cl_2) *δ* 10.25 (q, 1H, $^{4}J_{H\text{-}P}$ = 11.6), 7.52−7.49 (m, 3H), 7.41−7.37 (m, 9H), 7.29−7.22 (m, 9H), 7.06 (t, *J* = 9.0 Hz, 3H), 6.98 (t, *J* = 8.1 Hz, 6H), 6.73−6.62 (m, 9H), 6.38−6.36 (m, 3H), 2.07 (s, 9H). **^{31}P{^{1}H} NMR** (162 Hz, CD_2Cl_2) *δ* 31.78 (s); **^{13}C NMR** (101 Hz, CD_2Cl_2) *δ* 139.4−139.3 (s, C), 137.0−136.9 (s, C), 133.2 (s, C), 131.4−130.9 (m, CH), 130.2 (s, CH), 129.7−129.6 (m, CH), 129.1−128.8 (m, CH), 123.1 (s, CH), 121.8 (s, CH), 119.8 (s, CH), 119.2 (s, C), 115.9 (s, CH), 37.9 (q, $^{3}J_{C\text{-}P}$ = 21.1 Hz, H–$\underline{C}_{sp3}$), 8.9 (s, CH_3), 2.2 (s, CH_3); **^{19}F{^{1}H} NMR** (376 Hz, CD_2Cl_2) *δ* – 78.52 (s). **HRMS** (ESI, MeOH): calculated for $[C_{64}H_{52}CuN_3P_3]^+$, [M-OTf]$^+$: 1018.2665; found: 1018.2664. **X-Ray** quality crystals were obtained by slow diffusion of *t*BuOMe into the solution of the **2** in CH_2Cl_2 at 23 ºC.

[HTIM(PPh$_2$)$_3$Cu]Cl (3). Yellow crystalline solid was obtained in 70% yield after recrystallization from CH_2Cl_2:hexane. **^{1}H NMR** (400 Hz, CD_2Cl_2) *δ* 11.20 (q, 1H, $^{4}J_{H\text{-}P}$ = 10.3), 7.62−7.58 (m, 6H), 7.49−7.48 (m, 3H), 7.32−7.29 (m, 3H), 7.18−7.15 (m, 6H), 7.03−6.98 (m, 6H), 6.66 (t, *J* = 5.9 Hz, 6H), 6.63 (dt, *J* = 4.7, 1.1 Hz, 3H), 6.34−6.27 (m, 9H), 2.14 (s, 9H); **^{31}P{^{1}H} NMR** (162 Hz, CD_2Cl_2) *δ* 29.70 (s); **^{13}C NMR** (101 Hz, CD_2Cl_2) *δ* 139.2 (s, C), 137.6 (s, C), 132.9 (s, C), 131.1 (s, CH), 130.2−129.8 (m, CH), 128.6 (s, CH), 128.4 (s, CH), 127.8 (s, CH), 121.9 (s, CH), 120.8 (s, CH), 118.7 (s, CH), 117.9 (s, C), 116.2 (s, CH), 36.2 (q, $^{3}J_{C\text{-}P}$ = 17.7 Hz, H–$\underline{C}_{sp3}$), 8.4 (s, CH_3). **HRMS** (ESI, MeOH): calculated for $[C_{64}H_{52}CuN_3P_3]^+$, [M-Cl]$^+$: 1018.2665; found: 1018.2648. **Elemental analysis** (%) calc. for $C_{64}H_{52}CuN_3P_3Cl$ C% 72.86, H% 4.97, N% 3.98; found C% 72.21, H% 5.11, N% 4.09. **X-Ray** quality crystals were obtained by slow diffusion of *t*BuOMe into the solution of the **3** in CH_2Cl_2 at 23 ºC.

[HTIM(PPh$_2$)$_3$Cu]I (4). Yellow crystalline solid obtained in 86% by recrystallization from CH_2Cl_2:hexane. **^{1}H NMR** (400 Hz, CD_2Cl_2) *δ* 11.46 (*q*, 1H, $^{4}J_{H\text{-}P}$ = 9.6), 7.67−7.66 (m, 6H), 7.52−7.50 (m, 3H), 7.33−7.31 (m, 3H), 7.18−7.15 (m, 6H), 7.02−6.97 (m, 6H), 6.64−6.57 (m, 9H), 6.25−6.15 (m, 9H), 2.23 (s, 9H); **^{31}P{^{1}H} NMR** (162 Hz, CD_2Cl_2) *δ* 25.89 (s); **^{13}C NMR** (101 Hz, CD_2Cl_2) *δ* 139.8 (s, C), 138.2−138.1 (m, C), 133.4 (s, C), 132.0−131.8 (m, CH), 130.6 (s, CH), 130.4−130.3 (m, CH), 129.3 (s, CH), 128.9 (s, CH), 128.3 (s, CH), 122.5 (s, CH), 121.4 (s, CH), 119.3 (s, CH), 118.5 (s, C), 116.9 (s, CH), 36.5 (q, $^{3}J_{C\text{-}P}$ = 16.8 Hz, H–$\underline{C}_{sp3}$), 8.9 (s, CH_3). **HRMS** (ESI, MeOH): calculated for $[C_{64}H_{52}CuN_3P_3INa]^+$, [M+Na]$^+$: 1168.1607; found: 1168.1616. **Elemental analysis** (%) calc. for $C_{64}H_{52}CuN_3P_3I$ C% 67.05, H% 4.57, N% 3.67; found C% 67.00, H% 4.61, N% 3.89. **X-Ray** quality crystals were obtained by slow diffusion of *t*BuOMe into the solution of the **4** in CH_2Cl_2 at 23 ºC.

[HTIM(P*i*Pr$_2$)$_3$CuMeCN]BF$_4$ (5). Yellow crystalline solid obtained in 85% by recrystallization from CH_2Cl_2:hexane. **^{1}H NMR** (400 Hz, CD_2Cl_2) *δ* 7.60−7.55 (m, 4H), 7.48−7.46 (m, 3H), 7.29−7.19 (m, 6H), 3.25 (dsept, *J* = 5.6, 1.9 Hz, 3H), 2.65 (sept, *J* = 5.6 Hz, 3H), 2.41 (s, 3H),

1.47 (s, 9H), 1.41−1.36 (m, 9H), 1.18−1.14 (m, 9H), 0.95−0.84 (m, 18H); **^{31}P{^{1}H} NMR** (162 Hz, CD_2Cl_2) *δ* 63.72 (s); **^{13}C NMR** (101 Hz, CD_2Cl_2) *δ* 140.2−140.0 (m, C), 137.8−137.7 (m, C), 132.8 (s, C), 123.9 (s, CH), 121.8 (s, CH), 119.9 (s, CH), 114.1 (s, CH), 41.5 (q, $^{3}J_{C\text{-}P}$ = 16.8 Hz), 30.1 (s, CH_3), 26.8 (s, CH_3), 22.2−22.0 (m, CH_3), 20.7−20.2 (m, CH_3), 19.6 (s, CH_3), 8.4 (s, CH_3), 3.1 (s, CH_3); **^{19}F{^{1}H} NMR** (376 Hz, CD_2Cl_2) *δ* – 149.02 (s). **HRMS** (ESI, MeOH): calculated for $[C_{64}H_{52}CuN_3P_3]^+$, $[M\text{-}MeCN\text{-}BF_4]^+$: 814.3604; found: 814.3606.

[HTIM(P*i*Pr$_2$)$_3$Cu]OTf (6). Yellow crystalline solid obtained in 86% by recrystallization from CH_2Cl_2:hexane. **^{1}H NMR** (400 Hz, CD_2Cl_2) *δ* 7.82 (q, 1H, $^{4}J_{H\text{-}P}$ = 4.1 Hz), 7.61−7.59 (m, 3H), 7.47−7.45 (m, 3H), 7.27−7.17 (m, 6H), 3.22 (dsept, *J* = 5.2, 2.1 Hz, 3H), 2.65 (sept, *J* = 5.2 Hz, 3H), 1.44 (s, 9H), 1.43−1.37 (m, 9H), 1.21−1.16 (m, 9H), 1.00−0.95 (m, 9H), 0.86−0.85 (m, 9H); **^{31}P{^{1}H} NMR** (162 Hz, CD_2Cl_2) *δ* 64.08 (s); **^{13}C NMR** (101 Hz, CD_2Cl_2) *δ* 140.3−140.2 (m, C), 138.4−138.3 (m, C), 132.9 (s, C), 123.7 (s, CH), 121.6 (s, CH), 119.9 (s, CH), 119.7 (s, C), 114.4 (s, CH), 41.6 (q, $^{3}J_{C\text{-}P}$ = 17.3 Hz), 29.8 (s, CH_3), 26.7 (s, CH_3),

22.1−21.8 (m, CH_3), 20.8−20.6 (m, CH_3), 20.1−19.8 (m, CH_3), 19.6 (s, CH_3), 8.9 (s, CH_3); **^{19}F{^{1}H} NMR** (376 Hz, CD_2Cl_2) *δ*– 78.52 (s). **HRMS** (ESI, MeOH): calculated for $[C_{64}H_{52}CuN_3P_3]^+$, $[M\text{-}OTf]^+$: 814.3604; found: 814.3578. **X-Ray** quality crystals were obtained by slow diffusion of *t*BuOMe into the solution of the **6** in CH_2Cl_2 at 23 ºC.

[HTIM(P*i*Pr$_2$)$_3$Cu]Cl (7). isolated as a yellow crystalline solid in 78% (67%) by recrystallization from CH_2Cl_2:hexane. **^{1}H NMR** (400 Hz, CD_2Cl_2) *δ* 8.05 (q, 1H, $^{4}J_{H\text{-}P}$ = 5.5 Hz), 7.64−7.62 (m, 3H), 7.47−7.44 (m, 3H), 7.26−7.15 (m, 6H), 3.26 (sept, *J* = 7.2 Hz, 3H), 2.61 (sept, *J* = 7.2 Hz, 3H), 1.53−1.47 (m, 9H), 1.46 (s, 9H), 1.23−1.17 (m, 9H), 1.05−1.00 (m, 9H), 0.93−0.87 (m, 9H); **^{31}P{^{1}H} NMR** (162 Hz, CD_2Cl_2) *δ* 62.80 (s); **^{13}C NMR** (101 Hz, CD_2Cl_2) *δ* 140.4−140.3 (m, C), 139.2−139.0 (m, C), 132.9 (s, C), 123.7 (s, CH), 121.2 (s, CH), 119.7 (s, CH), 118.9 (s, C), 114.4 (s, CH), 41.1 (q, $^{3}J_{C\text{-}P}$ = 17.5 Hz), 30.0 (s, CH_3), 26.9 (s, CH_3), 22.0−21.7 (m, CH_3), 20.7−20.6 (m, CH_3), 19.9−19.7 (m, CH_3), 8.9 (s, CH_3). **HRMS** (ESI, MeOH): calculated for $[C_{46}H_{64}ClCuN_3NaP_3]^+$, $[M+Na]^+$: 872.3190; found: 872.3186. **Elemental analysis** (%) calc. for $C_{46}H_{64}CuN_3P_3Cl$ C% 64.93, H% 7.58, N% 4.94; found C% 64.74, H% 7.37, N% 5.04. **X-Ray** quality crystals were obtained by slow addition of hexane into the solution of the **7** in CH_2Cl_2 at 23 ºC.

[HTIM(P*i*Pr$_2$)$_3$Cu]I (8). Yellow crystalline solid obtained in 82% by recrystallization from CH_2Cl_2:hexane. **^{1}H NMR** (400 Hz, CD_2Cl_2) *δ* 7.89 (q, 1H, $^{4}J_{H\text{-}P}$ = 5.4 Hz), 7.61−7.59 (m, 3H), 7.44−7.41 (m, 3H), 7.23−7.13 (m, 6H), 3.26 (sept, *J* = 7.9 Hz, 3H), 2.65 (sept, *J* = 7.9 Hz, 3H), 1.55−1.49 (m, 9H), 1.37 (s, 9H), 1.24−1.18 (m, 9H), 1.06−1.00 (m, 9H), 0.94−0.89 (m, 9H); **^{31}P{^{1}H} NMR** (162 Hz, CD_2Cl_2) *δ* 61.96 (s); **^{13}C NMR** (101 Hz, CD_2Cl_2) *δ* 140.5−140.3 (m, C), 139.6−139.3 (m, C), 133.0 (s, C), 123.1 (s, CH), 121.2 (s, CH), 119.7 (s, CH), 118.9 (s, C), 114.6 (s, CH), 40.7 (q, $^{3}J_{C\text{-}P}$ = 19.6 Hz), 29.9 (s, CH_3), 26.9 (s, CH_3), 21.7−21.5 (m, CH_3), 20.9−20.7 (m, CH_3), 20.3−19.9 (m, CH_3), 8.8 (s, CH_3). **HRMS** (ESI, MeOH): calculated for $[C_{46}H_{64}CuN_3P_3]^+$, $[M\text{-}I]^+$: 814.3604; found: 814.3588. **X-Ray** quality crystals were obtained by slow addition of hexane into the solution of the **7** in CH_2Cl_2 at 23 ºC.

Acknowledgements

We would like to thank the European Commission for the ERC-CG-2014-648304 (J.Ll.-F) project. We also thank the financial support from ICIQ Foundation and CELLEX Foundation through the CELLEX-ICIQ high throughput experimentation platform and the Starting Career Program is gratefully acknowledged. We also thank CERCA Programme (Generalitat de Catalunya) for financial support and MINECO (Severo Ochoa Excellence Accreditation 2014–2018; SEV-2013-0319) and MINECO project CTQ2014-52525-P.

Keywords: organometallic complexes • electron density maps • selective coordination • CO_2 reduction • DFT modelling

[1] J. d. P. Peter Atkins, **2008**, *ISBN: 0-1992-8095-9*.

[2] T. Steiner, *Angew. Chem. Int. Ed.* **2002**, *41*, 48-76.

[3] L. Brammer, *Dalton Trans.* **2003**, 3145-3157.

[4] W. Scherer, A. C. Dunbar, J. E. Barquera-Lozada, D. Schmitz, G. Eickerling, D. Kratzert, D. Stalke, A. Lanza, P. Macchi, N. P. M. Casati, J. Ebad-Allah, C. Kuntscher, *Angew. Chem. Int. Ed.* **2015**, *54*, 2505-2509.

[5] a) M. Brookhart, M. L. H. Green, *J. Organomet. Chem.* **1983**, *250*, 395-408; b) J. Y. Saillard, R. Hoffmann, *J. Am. Chem. Soc.* **1984**, *106*, 2006-2026; c) R. H. Crabtree, D. G. Hamilton, in *Advances in Organometallic Chemistry, Vol. 28* (Eds.: F. G. A. Stone, R. West), Academic Press, **1988**, pp. 299-338; d) A. D. Ryabov, *Chem. Rev.* **1990**, *90*, 403-424; e) A. J. Canty, G. van Koten, *Acc. Chem. Res.* **1995**, *28*, 406-413; f) D. Braga, F. Grepioni, E. Tedesco, K. Biradha, G. R. Desiraju, *Organometallics* **1997**, *16*, 1846-1856.

[6] A. Mukhopadhyay, S. Pal, *Eur. J. Inorg. Chem.* **2006**, *2006*, 4879-4887.

[7] M. Ciclosi, J. Lloret, F. Estevan, M. Sanau, J. Perez-Prieto, *Dalton Trans.* **2009**, 5077-5082.

[8] M. Ciclosi, J. Lloret, F. Estevan, P. Lahuerta, M. Sanaú, J. Pérez-Prieto, *Angew. Chem. Int. Ed.* **2006**, *45*, 6741-6744.

[9] N. P. Mankad, M. T. Whited, J. C. Peters, *Angew. Chem. Int. Ed.* **2007**, *46*, 5768-5771.

[10] S. E. Creutz, J. C. Peters, *J. Am. Chem. Soc.* **2014**, *136*, 1105-1115.

[11] a) H. Fong, J. C. Peters, *Inorg. Chem.* **2015**, *54*, 5124-5135; b) S. Xu, X. Li, S. Zhang, H. Sun, *Inorganica Chim. Acta* **2015**, *430*, 161-167; c) C. Tsay, J. C. Peters, *Chem. Sci.* **2012**, *3*, 1313-1318; d) C. Tsay, N. P. Mankad, J. C. Peters, *J. Am. Chem. Soc.* **2010**, *132*, 13975-13977; e) A. Takaoka, A. Mendiratta, J. C. Peters, *Organometallics* **2009**, *28*, 3744-3753.

[12] S. Bontemps, G. Bouhadir, P. W. Dyer, K. Miqueu, D. Bourissou, *Inorg. Chem.* **2007**, *46*, 5149-5151.

[13] a) K. L. Haas, K. J. Franz, *Chem. Rev.* **2009**, *109*, 4921-4960; b) R. F. Carbonaro, Y. B. Atalay, D. M. Di Toro, *Geochim. Cosmochim. Acta* **2011**, *75*, 2499-2511; c) K. Hegetschweiler, *Angew. Chem.* **1997**, *109*, 546-546.

[14] M. Shokeen, C. J. Anderson, *Acc. Chem. Res.* **2009**, *42*, 832-841.

[15] T. J. Wadas, E. H. Wong, G. R. Weisman, C. J. Anderson, *Curr. Pharm. Des.* **2007**, *13*, 3-16.

[16] P. J. Blower, J. S. Lewis, J. Zweit, *Nucl. Med. Biol.* **1996**, *23*, 957-980.

[17] R. Shintani, K. Nozaki, *Organometallics* **2013**, *32*, 2459-2462.
[18] C. Kleeberg, M. S. Cheung, Z. Lin, T. B. Marder, *Journal of the American Chemical Society* **2011**, *133*, 19060-19063.
[19] D. S. Laitar, P. Müller, J. P. Sadighi, *J. Am. Chem. Soc.* **2005**, *127*, 17196-17197.
[20] S. Bagherzadeh, N. P. Mankad, *J. Am. Chem. Soc.* **2015**, *137*, 10898-10901.
[21] L. J. Murphy, H. Hollenhorst, R. McDonald, M. Ferguson, M. D. Lumsden, L. Turculet, *Organometallics* **2017**, *36*, 3709-3720.
[22] R. D. Hancock, A. E. Martell, *Chem. Rev.* **1989**, *89*, 1875-1914.
[23] H. Sigel, D. B. McCormick, *Acc. Chem. Res.* **1970**, *3*, 201-208.
[24] L. Rulíšek, Z. Havlas, *J J. Am. Chem. Soc.* **2000**, *122*, 10428-10439.
[25] a) S. Juran, M. Walther, H. Stephan, R. Bergmann, J. Steinbach, W. Kraus, F. Emmerling, P. Comba, *Bioconjug. Chem.* **2009**, *20*, 347-359; b) P. Comba, S. Hunoldt, M. Morgen, J. Pietzsch, H. Stephan, H. Wadepohl, *Inorg. Chem.* **2013**, *52*, 8131-8143; c) P. Comba, M. Kubeil, J. Pietzsch, H. Rudolf, H. Stephan, K. Zarschler, *Inorg. Chem.* **2014**, *53*, 6698-6707; d) A. Roux, A. M. Nonat, J. Brandel, V. Hubscher-Bruder, L. J. Charbonnière, *Inorg. Chem.* **2015**, *54*, 4431-4444.
[26] D. Brasse, A. Nonat, *Dalton Trans.* **2015**, *44*, 4845-4858.
[27] A. Aloisi, J.-C. Berthet, C. Genre, P. Thuery, T. Cantat, *Dalton Trans.* **2016**, *45*, 14774-14788.
[28] J. P. Foster, F. Weinhold, *J. Am. Chem. Soc.* **1980**, *102*, 7211-7218.
[29] a) W. Yao, O. Eisenstein, R. H. Crabtree, *Inorganica Chim. Acta* **1997**, *254*, 105-111; b) M. J. Calhorda, *Chem. Comm.* **2000**, 801-809.
[30] a) N. K. Hansen, P. Coppens, *Act. Cryst. A* **1978**, *34*, 909-921; b) C. Jelsch, B. Guillot, A. Lagoutte, C. Lecomte, *J. Appl. Crystallogr.* **2005**, *38*, 38-54.
[31] F. H. Allen, I. J. Bruno, *Act. Cryst. B* **2010**, *66*, 380-386.
[32] Rigaku, **2013**.
[33] G. M. Sheldrick, **2014**.
[34] M. C. Burla, R. Caliandro, B. Carrozzini, G. L. Cascarano, C. Cuocci, C. Giacovazzo, M. Mallamo, A. Mazzone, G. Polidori, *J. Appl. Crystallogr.* **2015**, *48*, 306-309.
[35] C. B. Hubschle, G. M. Sheldrick, B. Dittrich, *J. Appl. Crystallogr.* **2011**, *44*, 1281-1284.

Published in

European Journal of Inorganic Chemistry, *2018* (23), 2607-2607.

doi.org/10.1002/ejic.201800074